ACS OMEGA

Open Access

http://pubs.acs.org/journal/acsodf

Article

3D-Printed Cyclodextrin Polymer Encapsulated Wells–Dawson: A Novel Catalyst for Knoevenagel Condensation Reactions

Samahe Sadjadi,* Amir Masood Rezadoust,* Soheila Yaghoubi, Eric Monflier, and Abolfazl Heydari

Cite This: *ACS Omega* 2023, 8, 45844–45853

Read Online

ACCESS | Metrics & More | Article Recommendations

ABSTRACT: In the pursuit of enhancing the catalytic potential of the Wells–Dawson (WD) polyoxometalate (POM) while addressing its solubility challenges, this study focuses on devising a sustainable catalyst that operates effectively in aqueous environments. Leveraging cyclodextrin (CD) polymer chemistry in conjunction with 3D printing technology, a CD nanosponge, recognized for its interaction with POMs and molecular shuttle attributes, is synthesized as a scaffold for WD immobilization. Through integration into a 3D-printed monolith framework, the supported WD species becomes embedded within the catalyst structure, facilitating its application. Extensive characterization encompassing X-ray diffraction, thermogravimetric analysis, Fourier transform infrared, scanning electron microscopy/energy-dispersive system, elemental mapping analysis, and compression testing confirms the structural integrity and viability of the resulting catalyst. The catalytic assessment of the developed catalyst in the Knoevenagel condensation reaction within aqueous settings demonstrates enhanced reusability attributed to the encapsulation within the 3D matrix. Notably, a hot filtration test provides empirical evidence of heterogeneous catalysis mode, further underpinning the catalyst's performance and potential for sustainable applications.

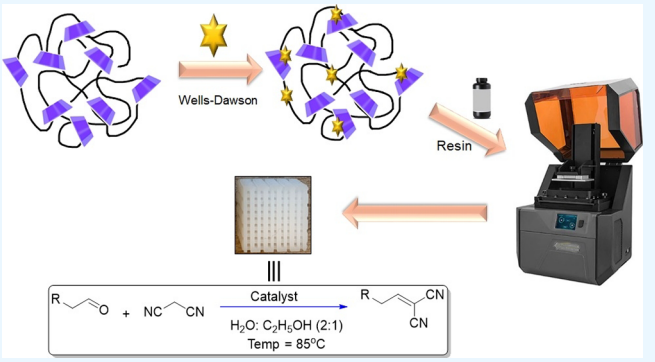

1. INTRODUCTION

Polyoxometalates (POMs) are soluble well-ordered anionic metal–oxygen clusters[1] with general formula of $[MOx]_n$, where M = Mo, Nb, W, Ta, V, and x = 4–7.[2] POMs benefit from a number of outstanding features, such as strong Bronsted acidity, high electronegativity, redox properties, and high chemical and thermal stability,[3] which expand their applications in various research areas, including catalysis,[4] sensors, fuel cells,[5] biochemistry, and chemical analysis.[5,6] One of the subclasses of POMs is heteropolyanions, which consist of heteroanions and are mostly applied for catalytic purposes. The most well-known heteropolyanions are Keggin $[XM_{12}O_{40}]^{n-}$ and Wells–Dawson (WD) anions $[X_2M_{18}O_{62}]^{n-}$ (where M = W or Mo; X = P, Si).[7] WD is an active and efficient catalytic species both for acid-catalyzed and redox chemical transformations.[8] One of the most well-known organic reactions that can be catalyzed with POM is the Knoevenagel condensation reaction.[9] As this is a key reaction for the synthesis of other chemicals, many attempts have been dedicated to develop efficient catalysts, such as Si-substituted polyoxovanadates,[10] chitosan nanofiber,[11] porous zeolite imidazolate framework,[12] that can promote it under mild reaction conditions

Similar to most POMs, the main challenge of WD is its high solubility in conventional solvents that renders its recovery and reuse arduous. To circumvent this issue, POMs have been heterogenized through stabilization on biobased and synthetic supports[13] or encapsulation within porous compounds.[14] In this context, the utilization of biobased supports, such as cyclodextrin (CD) and its polymers, has garnered significant attention. A distinguishing characteristic of CD is its cone-shaped structure, which imparts a hydrophilic outer surface and a hydrophobic cavity[15,16] and allows CD to act as a molecular shuttle for embedding hydrophobic guests in its cavity and transferring them in hydrophilic media.[16,17] CD also can form self-assembled systems, which have a broad range of applications.[18] CD-based polymers, such as CD nanosponges (CDNS),[19] also benefit from CD cavity effect,[20] and have demonstrated successful applications in catalysis. In fact, the use of nonsoluble CDNS with porous structures with diverse pore sizes is beneficial for stabilizing various catalytic species. Considering the role of CD and CDNS as phase-transfer

Received: September 1, 2023
Revised: October 5, 2023
Accepted: November 1, 2023
Published: November 20, 2023

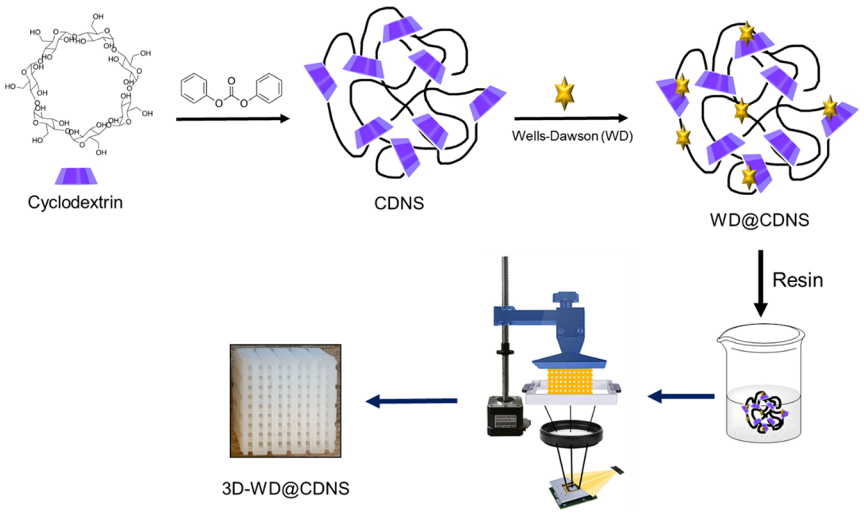

Figure 1. Pictorial procedure for the preparation of 3D-WD@CDNS.

catalysts, they are mostly designed for performing the reaction in aqueous media and developing environmentally benign protocols. According to the literature,[21] CDs can interact with POMs to form host–guest complexes or CD-POM-based frameworks. This feature makes it a potential support for the immobilization of various types of POMs. It is worth noting that for highly soluble catalysts, such as WD, there is always the possibility of catalyst leaching during the course of the reaction, potentially resulting in a decrease in the catalyst recyclability. While various solutions, including chemical and physical treatments of the support, have been proposed, this issue remains a challenging topic within the realm of heterogeneous catalysis.

An emerging approach for enhancing catalyst properties involves 3D printing.[22] In 3D printing, structures can be designed in freeform configurations based on digital models, and fluid/chemical engineering simulations can be harnessed for this purpose. This integration enables the comprehensive utilization of 3D printing in engineering, facilitating optimization of the structural design. Such optimization can significantly impact mass transfer and pressure drop within the catalyst, ultimately leading to enhanced catalytic performance.[23] In this context, numerous catalysts and electro- and photocatalysts have been previously documented. As an illustrative instance, Chatre et al.[24] devised a simplified methodology for structure-directed random packing, aimed at enhancing gas–liquid interfacial area and mitigating pressure drop. This approach involved the utilization of 3D-printed structures enveloped by randomly packed spherical particles. Recently, a novel methodology has been proposed by Franchi et al. for the evaluation of the mass transfer properties of 3D-printed catalyst supports. The 3D-printed samples were manufactured using a lab-scale stereolithography 3D printer, which was lower in cost and more accurate than equivalent metallic structures.[25] As reported by Han et al.,[26] the photosolid 3D printing method demonstrated the capability to directly fabricate Ni-based electrocatalysts characterized by distinctive gluten-like cubic structures. Additionally, in a straightforward electroless plating-baking process, a novel integrated 3D hollow foam electrode was engineered, which exhibited competence in operating at high current densities for water-related applications.[27]

The classification of 3D printing encompasses material extrusion-based, vat photopolymerization-based, and powder-based techniques, each category comprising various established methods.[28] Notably, digital light processing (DLP) stands out as a promising and straightforward approach for catalyst fabrication. DLP employs a light source, typically a projector, to solidify a photopolymer resin, thus offering a viable route for catalyst synthesis. Two technologies are used in this approach: (i) indirect, whereby a template is created, printed from a polymer resin, filled with the appropriate mixture, and finally burned out, or (ii) direct, wherein the polymer resin is mixed with other components, such as alumina, silica, hydroxyapatite, or zirconium.[29]

Building upon our ongoing exploration of heterogeneous catalysts[30,31] and POMs,[32] we present a novel approach that combines 3D printing technology with CDNS chemistry to address the challenge of leaching associated with WD-type POMs, while concurrently developing a proficient heterogeneous catalyst. In this context, we detail a comprehensive methodology involving the immobilization of WD onto CDNS, followed by the 3D printing process to produce a resilient catalyst denoted as 3D-WD@CDNS. Subsequently, we delve into the assessment of the catalytic performance and reusability of 3D-WD@CDNS within the context of the Knoevenagel condensation reaction, serving as a representative model for acid-catalyzed reactions.

2. EXPERIMENTAL SECTION

2.1. Materials. Diphenyl carbonate (DPC, 99%), β-cyclodextrin hydrate (CD, ≥97%), and ethanol (EtOH, >99%) were purchased from Sigma-Aldrich for the synthesis of CDNS. WD heteropolyacid ($H_6P_2W_{18}O_{62}$) was prepared according to the procedure described elsewhere.[33] For 3D printing, epoxyacrylate resin was supplied by ManPolymer Co., Iran.

2.2. Synthesis of WD@CDNS. CDNS was first prepared according to our previous report.[31] In brief, 16 mmol of DPC was melted and vigorously mixed with 2 mmol of CD at 120 °C, resulting in the formation of a white solid. The reaction was allowed to proceed for 20 h, after which the CDNS solid was manually crushed into a fine powder. To purify CDNS, we underwent sequential washing with deionized water and acetone. Subsequently, the precipitate was dried and subjected

https://doi.org/10.1021/acsomega.3c06592
ACS Omega 2023, 8, 45844−45853

to further purification via Soxhlet extraction with ethanol for a duration of 4 h.

To stabilize WD on CDNS, we employed the conventional wet impregnation method, as outlined in our previous work.[32] Specifically, we dissolved WD (20 wt %) in 5 mL of deionized water and gradually introduced it into a stirring suspension containing 1 g of CDNS in deionized water. The resulting mixture was stirred at 70 °C for 24 h to ensure the homogeneous stabilization of WD on CDNS. Following this, the solid was separated, subjected to multiple washes with deionized water, and subsequently dried at ambient temperature overnight.

2.3. Ink Preparation. The WD@CDNS ink was prepared by mixing 2 g of WD@CDNS powder with 2 g of acrylic resin. A high particle loading and low agglomeration slurry was created using an in-house micro pin mill. To achieve a 10 wt % suspension of WD@CDNS particles, an adequate amount of resin was added, followed by ultrasonication to ensure improved dispersion.

2.3.1. Printing of WD@CDNS: Preparation of 3D-WD@CDNS. A DLP 3D printer (Photon Ultra, Anycubic Ltd., China) was utilized for the fabrication of crosshatch structures under specified parameters: a 50 μm thickness, 60 s exposure time for the initial four layers, and 4 s exposure time for the subsequent layers. This process involved the dispensing of the suspension into a DLP 3D printer tank, followed by its uniform application onto a polymer sheet. Subsequently, the built plate was lowered and an ultraviolet projector was employed to cure the suspension onto the plate. Afterward, the built plate was raised and a coating was applied for the next layer, resulting in the formation of cubic crosshatch structures. To ensure the completion of the curing reaction and enhance mechanical properties, the 3D-printed crosshatch structure with dimensions of 1 × 1 cm^2 was transferred to a UV box for a 30 min exposure. The schematic procedure for the synthesis of 3D-WD@CDNS is depicted in Figure 1.

2.4. Characterization of 3D-WD@CDNS. Thermal stability of WD@CDNS, resin, and 3D-WD@CDNS was studied by thermogravimetric analysis using Mettler Toledo thermal calorimeter, in which the heating was performed under an oxygen atmosphere with a temperature increase of 10 °C min^{-1}. X-ray diffraction (XRD) patterns of WD@CDNS and 3D-WD@CDNS were obtained using Siemens, D5000 equipped with a Cu Kα radiation. The morphological study was conducted by scanning electron microscopy (SEM) using VEGAII TESCAN scanning electron microscope, equipped with QX2, RONTEC energy-dispersive X-ray analyzer. Fourier transform infrared (FTIR) spectra of WD@CDNS, resin, and 3D-WD@CDNS were recorded on PERKIN-ELMER-Spectrum 65 device (scan time of 1 s and spectral resolution of 2 cm^{-1}, using KBr pellet). Mechanical properties of the 3D-printed crosshatch structures were determined using a SANTAM STM-20 universal testing machine. The travel speed of the machine compressive testing plates was set to 5 mm·min^{-1}. A total of three specimens, each with dimensions of 1 cm × 1 cm, were subjected to compression testing.

2.5. Knoevenagel Condensation Reaction. The Knoevenagel condensation reaction, which is a useful organic transformation for the synthesis of organic compounds, was selected as a model chemical reaction to study the catalytic activity and recyclability of 3D-WD@CDNS. To conduct this reaction, malononitrile (11 mmol) and aldehyde (10 mmol) were dissolved in the mixture of deionized water and EtOH (2:1 w/w %) and then 3D-WD@CDNS was immersed in the solution, which was shaken. The temperature was elevated to 85 °C, and the progression of the reaction was monitored through thin-layer chromatography. After the reaction was completed, 3D-WD@CDNS was extracted, and the final product was obtained following solvent evaporation and silica gel column chromatography using a petroleum ether/EtOAc eluent (5:1 ratio).

2.6. Catalyst Recovery. In order to recycle the used 3D-WD@CDNS, it was immersed in acetone for 1 h using a shaker (150 rpm). The recovered 3D-WD@CDNS was subsequently dried at room temperature and employed for a subsequent reaction run.

3. RESULTS AND DISCUSSION

3.1. Characterization of 3D-WD@CDNS. The structures of WD@CDNS and 3D-WD@CDNS were analyzed by using XRD. It is well-established that CDNS, prepared through the aforementioned procedure, exhibits an amorphous nature, characterized by a broad peak in its XRD pattern within the 2θ range of 15−30°.[31] The XRD pattern of WD@CDNS is consistent with an amorphous structure, displaying no distinctive peaks corresponding to WD (Figure 2). According

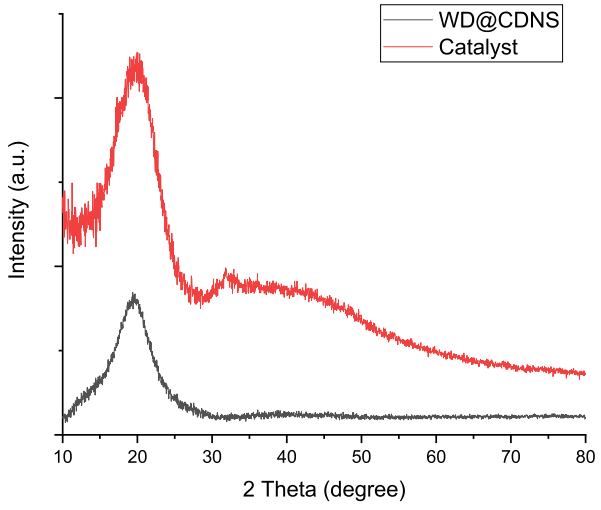

Figure 2. XRD patterns of WD@CDNS and the catalyst.

to the literature,[34] the absence of characteristic WD peaks can be attributed to its low loading and uniform distribution within the composite. As anticipated, the XRD pattern of 3D-WD@CDNS, primarily derived from an amorphous resin, similarly exhibits a broad peak indicative of its amorphous structural nature (Figure 2).

To gain further insight into the structure of 3D-WD@CDNS, we recorded its FTIR spectrum and compared it with those of the resin and WD@CDNS, as depicted in Figure 3. In the WD@CDNS spectrum, the absorbance bands at 3998, 2920, 1647, and 1746 cm^{-1} are representative of −OH, $-CH_2$, −C−O, and −C=O functionalities in CDNS, respectively. Furthermore, the bands appeared at 1152 cm^{-1} ($P-O_a$), 938 cm^{-1} ($W=O_d$), 865 cm^{-1} ($W-O_b-W$), and 755 cm^{-1} ($W-O_c-W$) can be ascribed to WD.[35] Concerning the FTIR spectrum of the commercial resin utilized for 3D printing, the absorbance band at 3427 cm^{-1} indicates the presence of the −OH functionality. Moreover, the bands observed at 2858 and 2966 cm^{-1} are representative of the $-CH_2$ bonds. The sharp

https://doi.org/10.1021/acsomega.3c06592
ACS Omega 2023, 8, 45844−45853

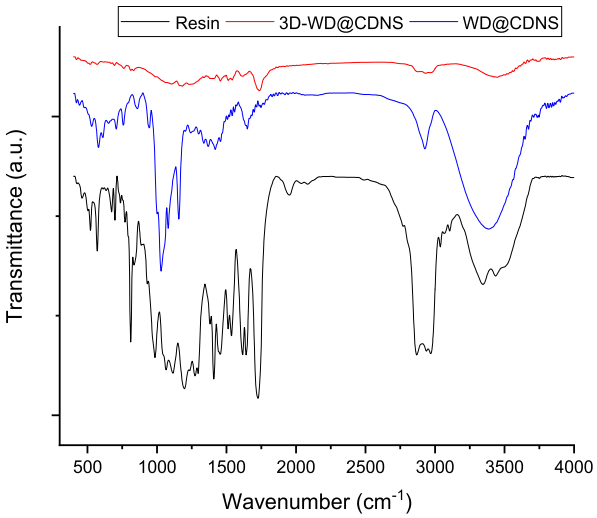

Figure 3. FTIR spectra of resin, WD@CDNS, and 3D-WD@CDNS.

bands at 1617 and 1726 cm^{-1} can be attributed to −C=C and −C=O functionality, respectively. FTIR spectrum of 3D-WD@CDNS exhibited the aforesaid characteristic bands of WD@CDNS. However, as some bands of WD@CDNS and resin overlapped.

In order to investigate both the catalyst morphology and the morphological impact of incorporating WD@CDNS on the 3D-printed structure, we compared SEM images of the WD@CDNS-free 3D-printed resin and 3D-WD@CDNS, as shown in Figure 4. As depicted in Figure 4A,D, the incorporation of WD@CDNS preserved the ordered structure of the 3D-printed resin. However, upon closer examination of the higher magnification images (Figure 4B,E), it became evident that WD@CDNS induced some degree of morphological alteration. Specifically, the WD@CDNS-free sample exhibited a well-ordered grooved surface, while the surface of 3D-WD@CDNS appeared nongrooved and adorned with small particles. This morphological distinction is more pronounced in Figure 4C,F, providing further confirmation of the incorporation of WD@CDNS within the 3D-printed structure.

To confirm the incorporation of WD@CDNS in the resulting 3D-printed structure, we conducted energy-dispersive system (EDS) analysis on 3D-WD@CDNS. As illustrated in Figure 5, 3D-WD@CDNS comprises C, W, and P atoms with C and O attributable to both CDNS and the resin. Additionally, the presence of P and W atoms confirms the presence of WD. Elemental mapping analysis of 3D-WD@CDNS, as shown in Figure 5, also demonstrates the nearly uniform dispersion of WD within the 3D-printed catalyst.

Thermal stability of the resin used for 3D printing, WD@CDNS, and 3D-WD@CDNS was also studied. As shown in

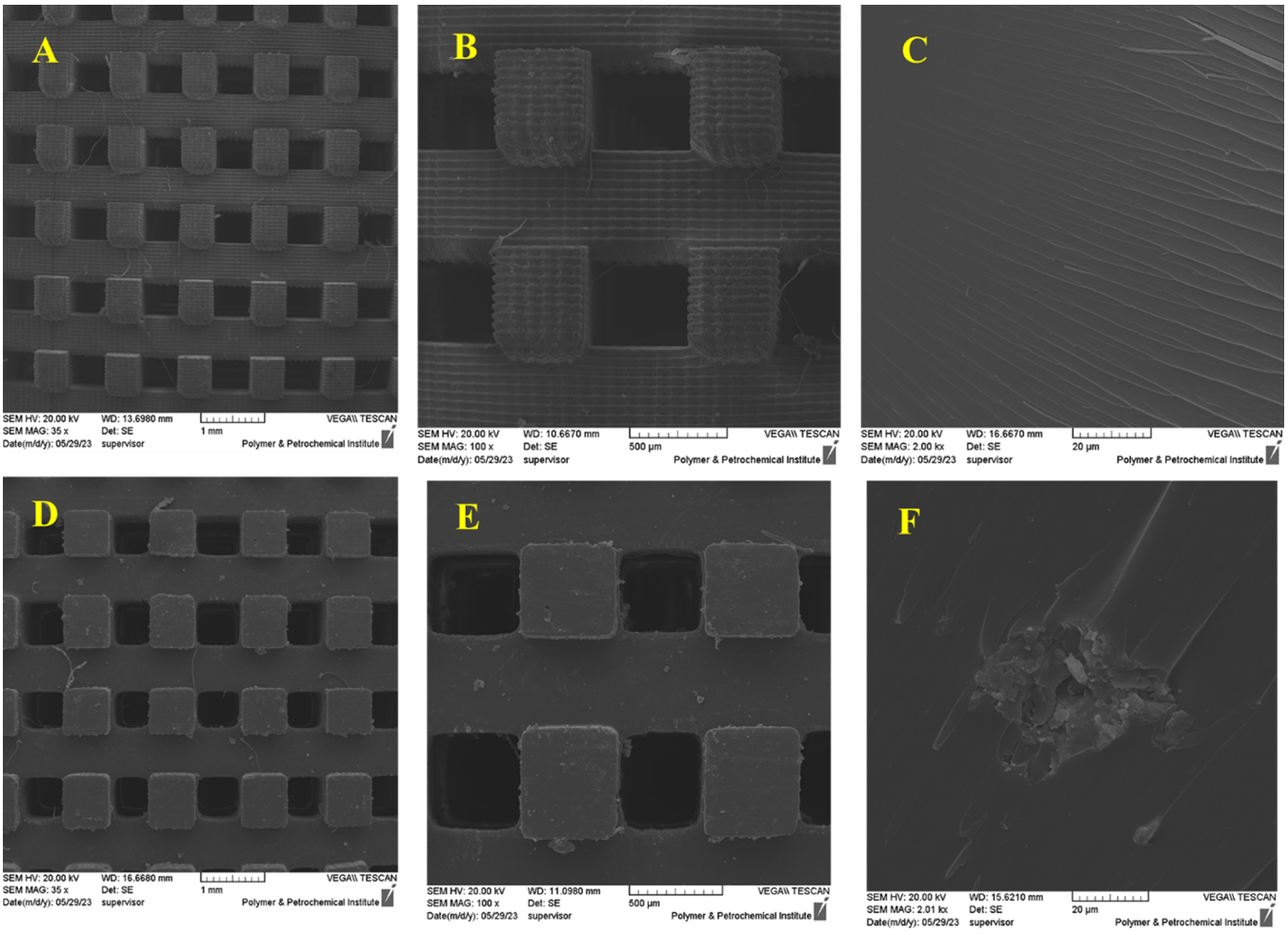

Figure 4. SEM images of 3D-printed resin (A−C) and 3D-WD@CDNS (D−F).

https://doi.org/10.1021/acsomega.3c06592
ACS Omega 2023, 8, 45844−45853

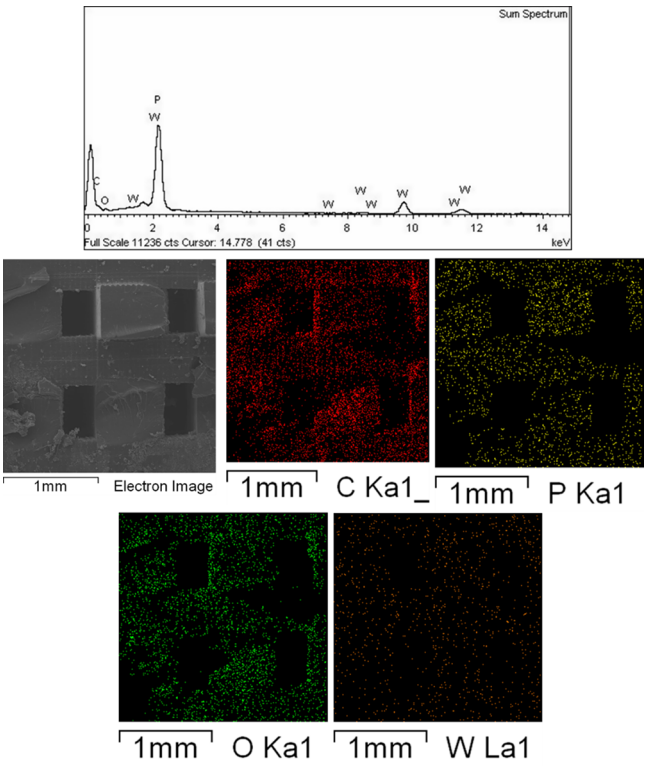

Figure 5. (Up) EDS and (down) elemental mapping analysis of the catalyst.

Figure 6, WD@CDNS thermogram is in good accordance with the previous reports[36] and exhibits one weight loss as a result

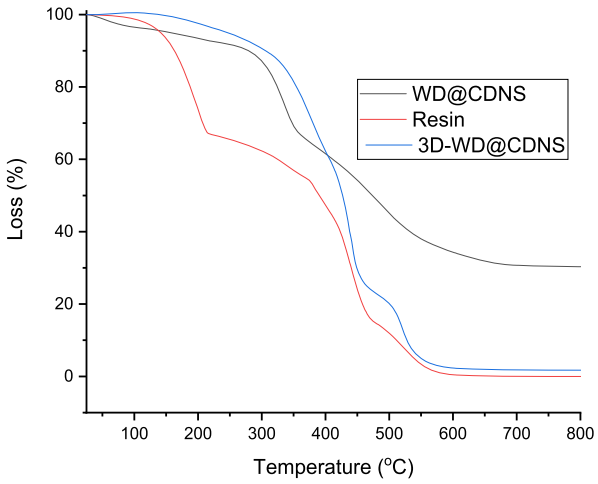

Figure 6. Thermograms of the resin, WD@CDNS, and 3D-WD@CDNS.

of evaporation of water (below 200 °C) and another one due to the decomposition of CDNS and WD, which occurs at 340 °C. The thermogram of the commercial resin that was utilized for printing showed three weight losses, one at 200 °C (removal of moisture) and two at ∼440 and 530 °C, which are related to the degradation of the resin. Regarding 3D-WD@CDNS, three weight losses at 380, ∼440, and 530 °C were detected that are ascribed to the decomposition of WD@CDNS and resin.

A compression test conducted on the 3D-printed structure revealed a compressive strength of 137 ± 20 MPa. This finding suggests that the structure possesses ample strength as a catalyst base and can withstand conventional mechanical forces. Moreover, it is noteworthy that the printed structure exhibits good homogeneity.

The results of XPS analysis of 3D-WD@CDNS are shown in Figure 7. The full scan XPS spectra of the nanocomposite, Figure 7a, contain the peaks of C 1s and O 1s. As shown in Figure 7b, high-resolution C 1s spectrum can be deconvoluted into the peak at 286.4, 286.7, and 292.5 eV that are respectively attributed to C−O, C−C, C=C, or C=O in the structure of resin and CDNS.[37]

Analyzing the O 1s spectrum and the respective binding energies gives insights into the types of oxygen-containing species in 3D-WD@CDNS, Figure 7c. Gaussian subpeak appeared at 537.8 eV and is attributed to C−O or oxygen−hydrogen (O−H) bonds.[38] It is worth noting that no peak related to WD, i.e., W and P, was observed. This issue can be due to the embedding of WD in the framework of the 3D-printed catalyst.

3.2. Optimization of the Reaction Conditions. To evaluate the catalytic performance of 3D-WD@CDNS, we chose the Knoevenagel condensation reaction between aldehydes and malononitrile, a pivotal organic transformation. Initially, we considered the reaction between benzaldehyde and malononitrile as a model Knoevenagel condensation reaction for the purpose of optimizing the reaction conditions.

3.2.1. Effect of Solvent. As described earlier, in pursuit of conducting the reaction in an aqueous environment, CDNS was employed as the support for WD. Consequently, we initially carried out the model reaction at 65 °C in water as the solvent. The results, shown in Table 1, revealed that under the aforementioned conditions, the desired product was obtained in a yield of 50%. Replacement of water with EtOH led to the increase of the yield of the reaction to 57%. Interestingly, the use of a mixture of these two solvents resulted in the improvement of the reaction yield, and the highest yield was achieved using H_2O/EtOH (2:1 v/v %). It is worth noting that conducting the reaction in some conventional solvents, such as acetonitrile, acetone, and CH_3Cl, was less efficient. Based on these findings, we selected a solvent mixture of H_2O/EtOH (2:1) for the subsequent experiments.

3.2.2. Effect of Reaction Temperature. We investigated the impact of the reaction temperature, a significant factor affecting the yield of the desired product. To achieve this, we conducted the model reaction across a temperature range spanning from 25 to 95 °C, and we quantified the product yield for each temperature variation, as depicted in Figure 8. The results clearly indicate that conducting the reaction at lower temperatures was inefficient, resulting in comparatively lower yields under these conditions. Upon raising the reaction temperature, however, the yield of the product was gradually increased and reached its maximum value of 87% at 85 °C. Importantly, increasing the temperature to 95 °C did not result in a significant impact on the reaction yield. As a consequence, the optimal reaction temperature was determined to be 85 °C. It is worth noting that under the optimum reaction conditions, no byproduct was detected.

3.3. Recyclability. WD is a catalytic species with high solubility in conventional solvents including water. Despite the potential of this catalyst to be stabilized on supporting materials, its propensity for leaching is notably pronounced,

https://doi.org/10.1021/acsomega.3c06592
ACS Omega 2023, 8, 45844−45853

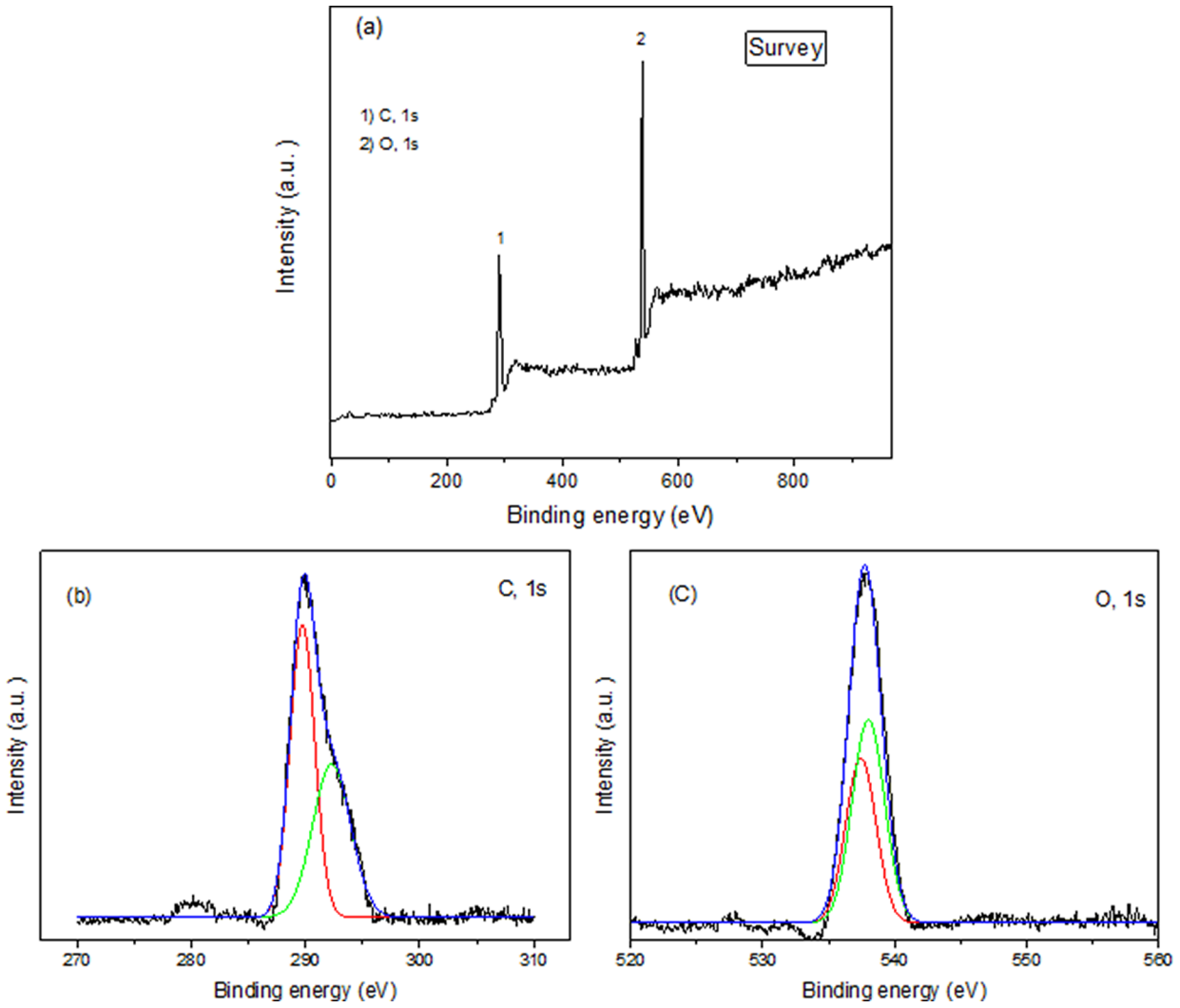

Figure 7. (a) Full scan XPS spectra of 3D-WD@CDNS, (b) C 1s, and (c) O 1s spectra.

Table 1. Effect of the Reaction Solvent on the Yield of the Model Reaction

entry	solvent	yield (%)
1	EtOH	57
2	H_2O	50
3	H_2O/EtOH (2:1)	65
4	H_2O/EtOH (1:1)	60
5	H_2O/EtOH (1:2)	58
6	acetone	45
7	CH_3Cl	48
8	CH_3CN	47

leading to unsatisfactory recyclability. In an effort to enhance this aspect of the catalyst, we initially stabilized WD on CDNS, resulting in WD@CDNS, which was subsequently encapsulated within a 3D-printed framework. The rationale behind this approach was the belief that embedding WD@CDNS within the 3D-printed structure could effectively suppress WD leaching, consequently improving catalyst recyclability. To assess this hypothesis, we investigated the recyclability of 3D-WD@CDNS in the model Knoevenagel condensation reaction under optimal reaction conditions. As shown in Figure 9, 3D-WD@CDNS preserved its catalytic activity for three successive runs and after that only insignificant loss of the catalytic

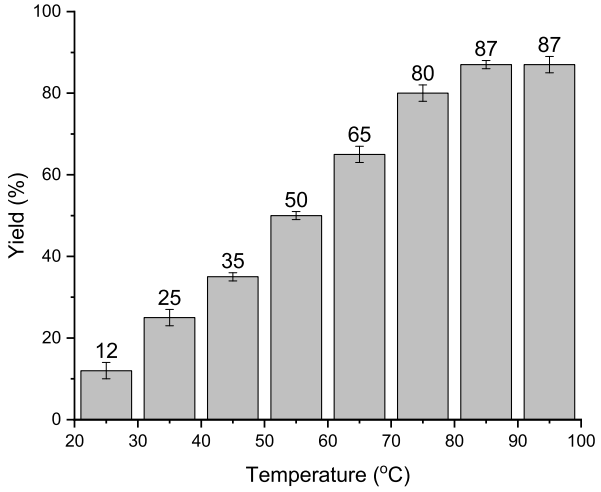

Figure 8. Investigation of the effect of the temperature on the yield of the model Knoevenagel condensation reaction.

activity (1%) was observed for the fourth and fifth reaction runs. For the sixth, seventh, and eighth runs, 4, 2, and 3% loss of the catalytic activity were observed, respectively. However,

https://doi.org/10.1021/acsomega.3c06592
ACS Omega 2023, 8, 45844−45853

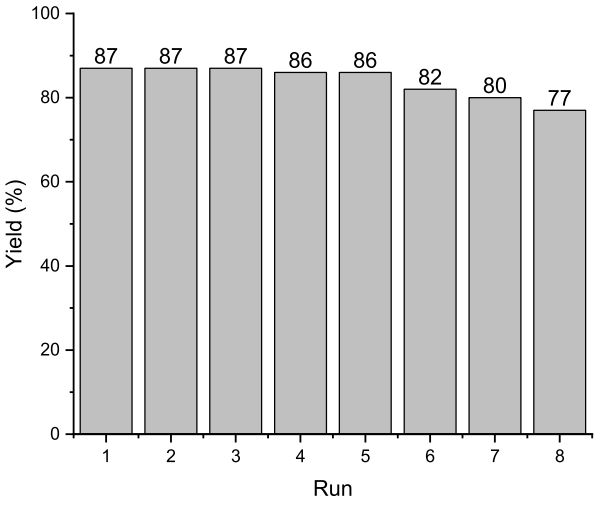

Figure 9. Recyclability of the as-prepared catalyst for the model Knoevenagel condensation reaction under the optimum reaction conditions, i.e., temperature: 85 °C, solvent: H_2O/EtOH (2:1).

the last run of the reaction resulted in 7% loss of activity. These results confirmed the high recyclability of 3D-WD@CDNS.

The substrates and products deposited on the recovered 3D-WD@CDNS were effectively removed through a washing procedure with acetone. To ascertain the stability of 3D-WD@CDNS upon recovery and recycling, we obtained the FTIR spectrum of the 3D-WD@CDNS after the seventh run of the model reaction and compared it with that of the fresh catalyst, as depicted in Figure 10. Gratifyingly, this comparison

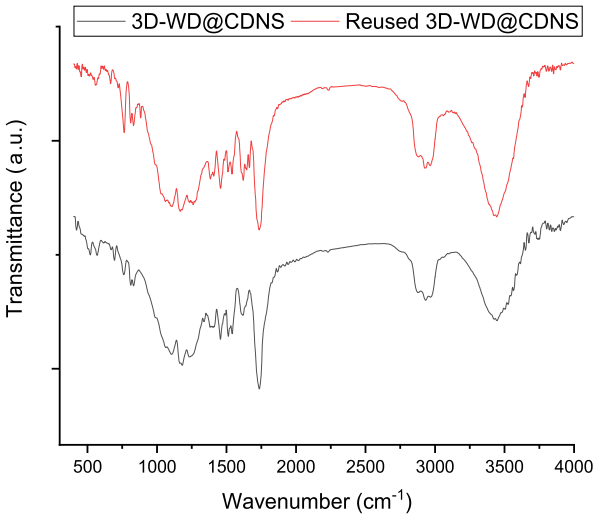

Figure 10. FTIR spectra of the fresh and reused 3D-WD@CDNS after the seventh Knoevenagel condensation reaction model under optimal reaction conditions.

confirmed the similarity of the two spectra, thereby establishing the structural stability of the recycled 3D-WD@CDNS. Furthermore, since no new absorbance bands emerged in the FTIR spectrum of the recycled catalyst, it can be concluded that simple washing was effective in removing deposited organic reagents.

3.4. Hot Filtration Test. Beyond recyclability, the authentic heterogeneity of a heterogeneous catalyst is a pivotal consideration. Indeed, in the case of WD, it can either be permanently anchored to the support or leach and subsequently redeposit during the Knoevenagel condensation reaction. To elucidate this matter, a hot filter test was conducted using the Knoevenagel condensation reaction model. To this aim, 3D-WD@CDNS was removed from the reaction vessel after a short reaction time (20 min), and the progress of the yield of the reaction was monitored for 4 h. The results, as depicted in Figure 11, indicated that in the

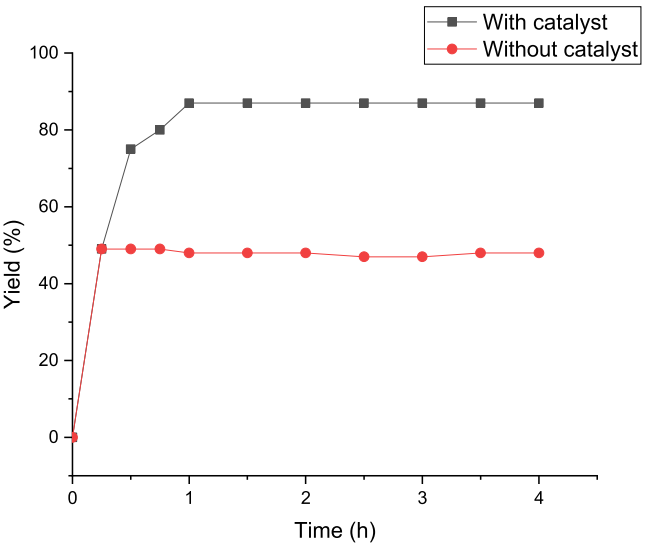

Figure 11. Results of the hot filtration test for the model Knoevenagel condensation reaction.

absence of 3D-WD@CDNS, the yield of the reaction did not increase, thereby ruling out the possibility of WD leaching during the course of the reaction and affirming the true heterogeneous nature of the catalysis.

3.5. Generality of the Developed Protocol. The results obtained from the model Knoevenagel condensation reaction involving benzaldehyde and malononitrile underscored the high activity of 3D-WD@CDNS under relatively mild reaction conditions. To assess the versatility of the developed protocol, various aldehydes, encompassing both aliphatic and aromatic aldehydes with electron-withdrawing and -donating groups, were utilized as substrates in conjunction with malononitrile. The outcomes, summarized in Table 2, substantiate that the nature of the substrate exerts a significant influence on the reaction yield, with less-active aliphatic aldehydes yielding lower results compared to their aromatic counterparts. Within the aromatic substrates, those bearing electron-withdrawing groups exhibited greater activity and produced higher yields.

4. CONCLUSIONS

The utilization of CDNS as a robust support for WD POM, resulting in the WD@CDNS composite, has been proven. By incorporating this composite into a 3D-printed framework, we successfully addressed concerns related to WD leaching, resulting in a catalytic monolith. Comprehensive characterization and application of this monolith in Knoevenagel condensation reactions revealed its versatility and efficiency. Importantly, the catalyst demonstrated remarkable recyclability due to the innovative 3D printing approach, ensuring sustained catalytic performance. The heterogeneous nature of the catalyst was unequivocally established through the hot filtration test, further affirming its effectiveness in heteroge-

https://doi.org/10.1021/acsomega.3c06592
ACS Omega 2023, 8, 45844−45853

Table 2. Knoevenagel Condensation Reaction of Various Aldehydes with Malononitrile Using 3D-WD@CDNS

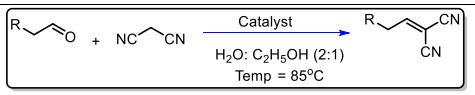

Entry	Substrate	Time (min)	Product	Yield%
1	Benzaldehyde	65	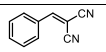	87
2	2-Nitrobezaldehyde	45	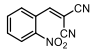	95
3	3-Chlorobenzaldehyde	50	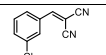	89
4	2,3-Dinitrobenzaldehyde	50	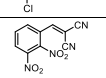	90
5	4-Chlorobenzaldehyde	60	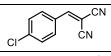	90
6	4-Aminobenzaldehyde	75	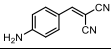	82
7	2-Hydroxybenzaldehyde	95	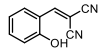	82
8	2-Methoxybenzaldehyde	125	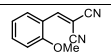	80
9	4-Methylbenzaldehyde	97	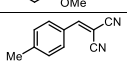	86
10	2-Methylpropanal	85	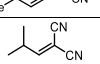	70
11	Formaldehyde	130	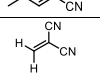	75
12	Propanal	130	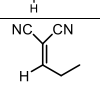	73
13	Furfural	150	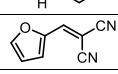	70

neous catalysis. This study underscores the potential of synergistic strategies involving CDNS support, 3D printing, and immobilization, offering a pathway to the development of recyclable and efficient catalytic systems for sustainable aqueous applications.

AUTHOR INFORMATION

Corresponding Authors

Samahe Sadjadi − *Gas Conversion Department, Faculty of Petrochemicals, Iran Polymer and Petrochemical Institute, Tehran 1497713-115, Iran; Center for International Scientific Studies & Collaboration (CISSC), Ministry of Science Research and Technology, Tehran 158757-788, Iran;* orcid.org/0000-0002-6884-4328; Email: s.sadjadi@ippi.ac.ir

Amir Masood Rezadoust − *Composites Department, Faculty of Petrochemicals, Iran Polymer and Petrochemical Institute, Tehran 1497713-115, Iran;* orcid.org/0000-0003-0198-0795; Email: A.Rezadoust@ippi.ac.ir

Authors

Soheila Yaghoubi − *Department of Chemistry, School of Physics and Chemistry, Alzahra University, Tehran 1993891-176, Iran*

Eric Monflier − *Univ. Artois, CNRS, Centrale Lille, Univ. Lille, UMR 8181, Unite de Catalyse et de Chimie du Solide (UCCS), Lens 62300, France;* orcid.org/0000-0001-5865-0979

Abolfazl Heydari − *Polymer Institute of the Slovak Academy of Sciences, Bratislava 845 41, Slovakia; Medical Vision, 821 08 Bratislava, Slovakia*

Complete contact information is available at: https://pubs.acs.org/10.1021/acsomega.3c06592

Notes

The authors declare no competing financial interest.

ACKNOWLEDGMENTS

This study was supported by the Center for International Scientific Studies and Collaboration (CISSC), Ministry of Science Research and Technology. The authors are also thankful to Iran Polymer and Petrochemical Institute for partial support. This work was supported by the Slovak Research and Development Agency under the contract numbers APVV-22-0568 and the Slovak Grant Agency VEGA 2/0121/23. This work is the result of the project implementation of Advanced bioactive hydrogel scaffolds for regenerative medicine (ABSACARM), ITMS2014+: 313011BWL6 supported by the Operational Programme Integrated Infrastructure funded by the European Regional Development Fund.

REFERENCES

(1) (a) Douvas, A. M.; Tsikritzis, D.; Tselios, C.; Haider, A.; Mougharbel, A. S.; Kortz, U.; Hiskia, A.; Coutsolelos, A. G.; Palilis, L. C.; Vasilopoulou, M.; et al. Multi-electron reduction of Wells−Dawson polyoxometalate films onto metallic, semiconducting and dielectric substrates. *Phys. Chem. Chem. Phys.* **2019**, *21* (1), 427−437. (b) Wang, X.; Rong, X.; Lin, H.; Cao, J.; Liu, G.; Chang, Z. A novel Wells−Dawson polyoxometalate-based metal−organic framework constructed from the uncommon in-situ transformed bi(triazole) ligand and azo anion. *Inorg. Chem. Commun.* **2016**, *63*, 30−34.

(2) (a) Wang, S.-S.; Yang, G.-Y. Recent Advances in Polyoxometalate-Catalyzed Reactions. *Chem. Rev.* **2015**, *115* (11), 4893−4962. (b) D'Cruz, B.; Amin, M. O.; Al-Hetlani, E. Polyoxometalate-Based Materials for the Removal of Contaminants from Wastewater: A Review. *Ind. Eng. Chem. Res.* **2021**, *60* (30), 10960−10977.

(3) Sadjadi, S.; Heravi, M. M. Recent Advances in Applications of POMs and Their Hybrids in Catalysis. *Curr. Org. Chem.* **2016**, *20*, 1404−1444.

(4) (a) da Silva Rocha, K. A.; Robles-Dutenhefner, P. A.; Kozhevnikov, I. V.; Gusevskaya, E. V. Phosphotungstic heteropoly acid as efficient heterogeneous catalyst for solvent-free isomerization of a-pinene and longifolene. *Appl. Catal., A* **2009**, *352*, 188−192. (b) Li, B.; Ma, W.; Han, C.; Liu, J.; Pang, X.; Gao, X. Preparation of MCM-41 incorporated with transition metal substituted polyoxometalate and its catalytic performance in esterification. *Microporous Mesoporous Mater.* **2012**, *156*, 73−79. (c) Alsalme, A. M.; Kozhevnikova, E. F.; Kozhevnikov, I. V. a-Pinene isomerisation over heteropoly acid catalysts in the gas-phase. *Appl. Catal., A* **2010**, *390*, 219−224. (d) Alsalme, A. M.; Wiper, P. V.; Khimyak, Y. Z.; Kozhevnikova, E. F.; Kozhevnikov, I. V. Solid acid catalysts based on H3PW12O40 heteropoly acid: Acid and catalytic properties at a gas−solid interface. *J. Catal.* **2010**, *276*, 181−189. (e) Amanchi, S.; Khenkin, A. M.; Diskin-Posner, Y.; Neumann, R. A Bismuth Substituted "Sandwich" Type Polyoxometalate Catalyst for Activation of Peroxide − Umpolung of the Peroxo Intermediate and Change of Chemoselectivity. *ACS Catal.* **2015**, *5*, 3336−3341. (f) Han, X.; Yan, W.; Chen, K.; Hung, C.-T.; Liu, L.-L.; Wu, P.-H.; Huang, S.-J.; Liu, S.-M. Heteropolyacid-based ionic liquids as effective catalysts for thesynthesis of benzaldehyde glycol acetal. *Appl. Catal., A* **2014**, *485*, 149−156. (g) Liu, M.; Deng, W.; Zhang, Q.; Wang, Y.; Wang, Y. Polyoxometalate-supported ruthenium nanoparticles as bifunctional heterogeneous catalysts for the conversions of cellobiose and cellulose

https://doi.org/10.1021/acsomega.3c06592
ACS Omega 2023, 8, 45844−45853

into sorbitol under mild conditions. *Chem. Commun.* **2011**, *47*, 9717−9719. (h) Micek-Ilnicka, A.; Bielanska, E.; Litynska-Dobrzynska, L.; Bielanski, A. Carbon nanotubes, silica and titania supported heteropolyacid H3PW12O40 as the catalyst for ethanol conversion. *Appl. Catal., A* **2012**, *421*−*422*, 91−98. (i) Nisar, A.; Lu, Y.; Zhuang, H.; Wang, X. Polyoxometalate Nanocone Nanoreactors: Magnetic Manipulation and Enhanced Catalytic Performance. *Angew. Chem.* **2011**, *123*, 3245−3250. (j) Nisar, A.; Wang, X. Surfactant-encapsulated polyoxometalate building blocks: controlled assembly and their catalytic properties. *Dalton Trans.* **2012**, *41*, 9832−9845. (k) Noro, S.-I.; Tsunashima, R.; Kamiya, Y.; Uemura, K.; Kita, H.; Cronin, L.; Akutagawa, T.; Nakamura, T. Adsorption and Catalytic Properties of the Inner Nanospace of a Gigantic Ring-Shaped Polyoxometalate Cluster. *Angew. Chem.* **2009**, *121*, 8859−8862. (l) Pasquale, G.; Vázquez, P.; Romanelli, G.; Baronetti, G. Catalytic upgrading of levulinic acid to ethyl levulinate using reusable silica-included Wells-Dawson heteropolyacid as catalyst. *Catal. Commun.* **2012**, *18*, 115−120. (m) Rafiee, E.; Shahebrahimi, S. Nano Silica with High Surface Area from Rice Husk as a Support for 12-Tungstophosphoric Acid: An Efficient Nano Catalyst in Some Organic Reactions. *Chin. J. Catal.* **2012**, *33*, 1326−1333. (n) Suzuki, K.; Sugawa, M.; Kikukawa, Y.; Kamata, K.; Yamaguchi, K.; Mizuno, N. Strategic Design and Refinement of Lewis Acid−Base Catalysis by Rare-Earth-Metal-Containing Polyoxometalates. *Inorg. Chem.* **2012**, *51*, 6953−6961. (o) Yadav, G. D.; Tekale, D. P. Selective mono-isopropylation of 1,3-propanediol with isopropylalcohol using heteropoly acid supported on K-10 clay catalyst. *Catal. Today* **2014**, *237*, 54−61.

(5) Kourasi, M.; Wills, R. G. A.; Shah, A. A.; Walsh, F. C. Heteropolyacids for fuel cell applications. *Electrochim. Acta* **2014**, *127*, 454−466.

(6) (a) Fileka, U.; Bielańska, E.; Socha, R. P.; Bielański, A. Reduced copper salt of Wells−Dawson type heteropolyacid as a bifunctional catalyst. *Catal. Today* **2011**, *169*, 150−155. (b) Heravi, M. M.; Sadjadi, S. Recent Developments in Use of Heteropolyacids, Their Salts and Polyoxometalates in Organic Synthesis. *J. Iran. Chem. Soc.* **2009**, *6*, 1−54.

(7) Long, D.-L.; Tsunashima, R.; Cronin, L. Polyoxometalates: Building Blocks for Functional Nanoscale Systems. *Angew. Chem., Int. Ed.* **2010**, *49* (10), 1736−1758.

(8) (a) Ghanbari, M.; Moradi, S.; Setoodehkhah, M. Fe3O4@SiO2@ADMPT/H6P2W18O62: a novel Wells−Dawson heteropolyacid-based magnetic inorganic−organic nanohybrid material as potent Lewis acid catalyst for the efficient synthesis of 1,4-dihydopyridines. *Green Chem. Lett. Rev.* **2018**, *11* (2), 111−124. (b) García-López, E. I.; Marcì, G.; Krivtsov, I.; Casado Espina, J.; Liotta, L. F.; Serrano, A. Local Structure of Supported Keggin and Wells−Dawson Heteropolyacids and Its Influence on the Catalytic Activity. *J. Phys. Chem. C* **2019**, *123* (32), 19513−19527. (c) Comuzzi, C.; Primavera, A.; Trovarelli, A.; Bini, G.; Cavani, F. Thermal stability and catalytic properties of the Wells-Dawson K6P2W18O62·10H2O heteropoly compound in the oxidative dehydrogenation of isobutane to isobutene. *Top. Catal.* **1996**, *3* (3), 387−406.

(9) Knoevenagel, E. Condensation von Malonsäure mit aromatischen Aldehyden durch Ammoniak und Amine. *Ber. Dtsch. Chem. Ges.* **1898**, *31* (3), 2596−2619.

(10) Shi, Y.; Zhou, T.; Di, J.-Q.; Wang, W.; Ma, L.; Zhang, H.; Gao, Y. Three Si-substituted polyoxovanadates as efficient catalysts for Knoevenagel condensation and selective oxidation of styrene to benzaldehyde. *Dalton Trans.* **2022**, *51* (8), 3304−3313.

(11) Hirayama, Y.; Kanomata, K.; Hatakeyama, M.; Kitaoka, T. Chitosan nanofiber-catalyzed highly selective Knoevenagel condensation in aqueous methanol. *RSC Adv.* **2020**, *10* (45), 26771−26776.

(12) Tran, U. P. N.; Le, K. K. A.; Phan, N. T. S. Expanding Applications of Metal−Organic Frameworks: Zeolite Imidazolate Framework ZIF-8 as an Efficient Heterogeneous Catalyst for the Knoevenagel Reaction. *ACS Catal.* **2011**, *1* (2), 120−127.

(13) (a) Ma, T.; Ding, J.; Shao, R.; Xu, W.; Yun, Z. Dehydration of glycerol to acrolein over Wells−Dawson and Keggin type phosphotungstic acids supported on MCM-41 catalysts. *Chem. Eng. J.* **2017**, *316*, 797−806. (b) Tayebee, R.; Amini, M. M.; Rostamian, H.; Aliakbari, A. Preparation and characterization of a novel Wells−Dawson heteropolyacid-based magnetic inorganic−organic nanohybrid catalyst H6P2W18O62/pyridino-Fe3O4 for the efficient synthesis of 1-amidoalkyl-2-naphthols under solvent-free conditions. *Dalton Trans.* **2014**, *43* (4), 1550−1563. (c) Ding, J.; Ma, T.; Shao, R.; Xu, W.; Wang, P.; Song, X.; Guan, R.; Yeung, K.; Han, W. Gas phase dehydration of glycerol to acrolein on an amino siloxane-functionalized MCM-41 supported Wells−Dawson type H6P2W18O62 catalyst. *New J. Chem.* **2018**, *42* (17), 14271−14280. (d) Amaya, J.; Moreno, S.; Molina, R. Heteropolyacids supported on clay minerals as bifunctional catalysts for the hydroconversion of decane. *Appl. Catal., B* **2021**, *297*, No. 120464.

(14) Zhang, Z.; Gómez-García, C. J.; Wu, Q.; Xin, J.; Pang, H.; Ma, H.; Chai, D.; Li, S.; Zhao, C. Synthesis of a Polyoxometalate-Encapsulated Metal−Organic Framework via In Situ Ligand Transformation Showing Highly Catalytic Activity in Both Hydrogen Evolution and Dye Degradation. *Inorg. Chem.* **2022**, *61* (30), 11830−11836.

(15) (a) Thanh Chau, N. T.; Handjani, S.; Guegan, J. P.; Guerrero, M.; Monflier, E.; Philippot, K.; Denicourt-Nowicki, A.; Roucoux, A. Methylated b-Cyclodextrin-Capped Ruthenium Nanoparticles: Synthesis Strategies, Characterization, and Application in Hydrogenation Reactions. *Chem. Catal. Chem.* **2013**, *5*, 1497−1503. (b) Manivannan, S.; Ramaraj, R. Synthesis of cyclodextrin-silicate sol−gel composite embedded gold nanoparticles and its electrocatalytic application. *Chem. Eng. J.* **2012**, *210*, 195−202. (c) Bleta, R.; Noël, S.; Addad, A.; Ponchela, A.; Monflier, E. Mesoporous RuO_2/TiO_2 composites prepared by cyclodextrin-assisted colloidal self-assembly: towards efficient catalysts for the hydrogenation of methyl oleate. *RSC Adv.* **2016**, *6*, 14570−14579.

(16) Noël, S.; Légera, B.; Ponchel, A.; Hapiot, F.; Monflier, E. Effective Catalytic Hydrogenation of Fatty Acids Methyl Esters by Aqueous Rhodium(0) Nanoparticles Stabilized by Cyclodextrin-Based Polymers. *Chem. Eng. Trans.* **2014**, *37*, 337−342.

(17) (a) Ozyilmaz, E.; Sayin, S.; Arslan, M.; Yilmaz, M. Improving catalytic hydrolysis reaction efficiency of sol−gel-encapsulated Candida rugosa lipase with magnetic β-cyclodextrin nanoparticles. *Colloids Surf., B* **2014**, *113*, 182−189. (b) Menuel, S.; Léger, B.; Addad, A.; Monflier, E.; Hapiot, F. Cyclodextrins as Effective Additives in AuNPs-Catalyzed Reduction of Nitrobenzene Derivatives in a Ball-Mill. *Green Chem.* **2016**, *18*, 5500−5509.

(18) (a) Calvino, M. M.; Lazzara, G.; Cavallaro, G.; Milioto, S. Inclusion complexes of triblock L35 copolymer and hydroxyl propyl cyclodextrins: a physico-chemical study. *New J. Chem.* **2022**, *46* (13), 6114−6120. (b) Guo, J.; Hou, J.; Hu, J.; Geng, Y.; Li, M.; Wang, H.; Wang, J.; Luo, Q. Recent advances in β-cyclodextrin-based materials for chiral recognition. *Chem. Commun.* **2023**, *59* (60), 9157−9166.

(19) (a) Matencio, A.; Guerrero-Rubio, M. A.; Caldera, F.; Cecone, C.; Trotta, F.; García-Carmona, F.; López-Nicolás, J. M. Lifespan extension in Caenorhabditis elegans by oxyresveratrol supplementation in hyper-branched cyclodextrin-based nanosponges. *Int. J. Pharm.* **2020**, *589*, No. 119862. (b) Matencio, A.; Dhakar, N. K.; Bessone, F.; Musso, G.; Cavalli, R.; Dianzani, C.; García-Carmona, F.; López-Nicolás, J. M.; Trotta, F. Study of oxyresveratrol complexes with insoluble cyclodextrin based nanosponges: Developing a novel way to obtain their complexation constants and application in an anticancer study. *Carbohydr. Polym.* **2020**, *231*, No. 115763. (c) Appleton, S. L.; Tannous, M.; Argenziano, M.; Muntoni, E.; Rosa, A. C.; Rossi, D.; Caldera, F.; Scomparin, A.; Trotta, F.; Cavalli, R. Nanosponges as protein delivery systems: Insulin, a case study. *Int. J. Pharm.* **2020**, *590*, No. 119888.

(20) (a) Silva, F.; Caldera, F.; Trotta, F.; Nerín, C.; Domingues, F. C. Encapsulation of coriander essential oil in cyclodextrin nanosponges: A new strategy to promote its use in controlled-release active packaging. *Innov. Food Sci. Emerg. Technol.* **2019**, *56*, No. 102177. (b) Pawar, S.; Shende, P.; Trotta, F. Diversity of β-cyclodextrin-based

https://doi.org/10.1021/acsomega.3c06592
ACS Omega 2023, 8, 45844−45853

nanosponges for transformation of actives. *Int. J. Pharm.* **2019**, *565*, 333−350.
(21) Khlifi, S.; Marrot, J.; Haouas, M.; Shepard, W. E.; Falaise, C.; Cadot, E. Chaotropic Effect as an Assembly Motif to Construct Supramolecular Cyclodextrin−Polyoxometalate-Based Frameworks. *J. Am. Chem. Soc.* **2022**, *144* (10), 4469−4477.
(22) (a) Kondapalli, V. K. R.; He, X.; Khosravifar, M.; Khodabakhsh, S.; Collins, B.; Yarmolenko, S.; Paz y Puente, A.; Shanov, V. CVD Synthesis of 3D-Shaped 3D Graphene Using a 3D-Printed Nickel−PLGA Catalyst Precursor. *ACS. Omega* **2021**, *6* (43), 29009−29021. (b) Lahtinen, E.; Turunen, L.; Hänninen, M. M.; Kolari, K.; Tuononen, H. M.; Haukka, M. Fabrication of Porous Hydrogenation Catalysts by a Selective Laser Sintering 3D Printing Technique. *ACS Omega* **2019**, *4* (7), 12012−12017.
(23) (a) Zhu, J.; Wu, P.; Chao, Y.; Yu, J.; Zhu, W.; Liu, Z.; Xu, C. Recent advances in 3D printing for catalytic applications. *Chem. Eng. J.* **2022**, *433*, No. 134341. (b) Gao, Y.; Lalevée, J.; Simon-Masseron, A. An Overview on 3D Printing of Structured Porous Materials and Their Applications *Adv. Mater. Technol.* **2023**, *8*, 2300377, . (c) Chen, J.; Wu, P.; Bu, F.; Gao, Y.; Liu, X.; Guan, C. 3D printing enhanced catalysis for energy conversion and environment treatment. *DeCarbon* **2023**, *2*, No. 100019.
(24) Chatre, L.; Socci, J.; Adams, S. J.; Denissenko, P.; Cherkasov, N. Design of 3D-printed structures for improved mass transfer and pressure drop in packed-bed reactors. *Chem. Eng. J.* **2021**, *420*, No. 129762.
(25) Franchi, F. S.; Ambrosetti, M.; Balzarotti, R.; Bracconi, M.; Groppi, G.; Tronconi, E. Rich H2 catalytic oxidation as a novel methodology for the evaluation of mass transport properties of 3D printed catalyst supports. *Catal. Today* **2022**, *383*, 123−132.
(26) Han, Z.; Wang, G.; Zhang, J.; Tang, Z. Direct photo-curing 3D printing of nickel-based electrocatalysts for highly-efficient hydrogen evolution. *Nano Energy* **2022**, *102*, No. 107615.
(27) Liu, H.; Li, X.; Chen, L.; Zhu, X.; Dong, P.; Chee, M. O. L.; Ye, M.; Guo, Y.; Shen, J. Monolithic Ni-Mo-B Bifunctional Electrode for Large Current Water Splitting. *Adv. Funct. Mater.* **2022**, *32* (4), No. 2107308.
(28) Chen, L.; Zhou, S.; Li, M.; Mo, F.; Yu, S.; Wei, J. Catalytic Materials by 3D Printing: A Mini Review. *Catalysts* **2022**, *12* (10), 1081.
(29) Nowakowska, M.; Rokicińska, A.; Kuśtrowski, P.; Michorczyk, P. Composite resins for 3D printing of corundum and corundum-kaolin based monoliths for catalytic applications. *Ceram. Int.* **2023**, *49* (2), 1902−1910.
(30) (a) Sadjadi, S.; Abedian-Dehaghani, N.; Zhong, X.; Heravi, M. M.; Yuan, P. Ionic liquid-functionalized halloysite as an efficient catalyst for the production of 5-hydroxymethylfurfural. *Appl. Clay Sci.* **2023**, *237*, No. 106896. (b) Sadjadi, S.; Abedian-Dehaghani, N.; Heravi, M. M.; Zhong, X.; Yuan, P.; Duran, J.; Poater, A.; Bahri-Laleh, N. Clay-supported acidic ionic liquid as an efficient catalyst for conversion of carbohydrates to 5-hydroxymethylfurfural. *J. Mol. Liq.* **2023**, *382*, No. 121847.
(31) Sadjadi, S.; Koohestani, F. Palladated composite of MOF and cyclodextrin nanosponge: A novel catalyst for hydrogenation reaction. *J. Mol. Struct.* **2021**, *1245*, No. 131068.
(32) Abedian-Dehaghani, N.; Sadjadi, S.; Heravi, M. M. Heteropoyacid on the composite of boehmite and polyionic liquid as a catalyst for alcohol oxidation and tandem alcohol oxidation Knoevenagel condensation reactions. *Sci. Rep.* **2022**, *12* (1), 16395.
(33) Marcì, G.; García-López, E. I.; Pomilla, F. R.; Liotta, L. F.; Palmisano, L. Enhanced (photo)catalytic activity of Wells-Dawson (H6P2W18O62) in comparison to Keggin (H3PW12O40) heteropolyacids for 2-propanol dehydration in gas-solid regime. *Appl. Catal. A: Gen.* **2016**, *528*, 113−122.
(34) Mallik, S.; Dash, S. S.; Parida, K. M.; Mohapatra, B. K. Synthesis, characterization, and catalytic activity of phosphomolybdic acid supported on hydrous zirconia. *J. Colloid Interface Sci.* **2006**, *300*, 237−243.
(35) Bielański, A.; Lubańska, A. FTIR investigation on Wells−Dawson and Keggin type heteropolyacids: dehydration and ethanol sorption. *J. Mol. Catal. A Chem.* **2004**, *224* (1), 179−187.
(36) Sadjadi, S.; Heravi, M. M.; Malmir, M. Pd@HNTs-CDNS-g-C_3N_4: a novel heterogeneous catalyst for promoting ligand and copper-free Sonogashira and Heck coupling reactions, benefits from halloysite and cyclodextrin chemistry and g-C_3N_4 contribution to suppress Pd leaching. *Carbohydr. Polym.* **2018**, *186*, 25−34.
(37) (a) Mohtasebi, A.; Chowdhury, T.; Hsu, L. H.; Biesinger, M. C.; Kruse, P. Interfacial charge transfer between phenyl-capped aniline tetramer films and iron oxide surfaces. *J. Phys. Chem. C* **2016**, *120* (51), 29248−29263. (b) Sun, J.; Gao, A.; Wang, X.; Xu, X.; Song, J. Removal of Phosphorus from Wastewater by Different Morphological Alumina. *Molecules* **2020**, *25* (13), 3092.
(38) (a) Al-Gaashani, R.; Zakaria, Y.; Lee, O.-S.; Ponraj, J.; Kochkodan, V.; Atieh, M. A. Effects of preparation temperature on production of graphene oxide by novel chemical processing. *Ceram. Int.* **2021**, *47* (7), 10113−10122. (b) Li, Y. G.; Quan, X.; Hu, C.; Li, C. Effective Catalytic Reduction of 4-Nitrophenol to 4-Aminophenol over Etched Halloysite Nanotubes@α-Ni(OH)2. *ACS Appl. Energy Mater.* **2020**, *3* (5), 4756−4766.

https://doi.org/10.1021/acsomega.3c06592
ACS Omega 2023, 8, 45844−45853